Hindawi Publishing Corporation
Advances in Materials Science and Engineering
Volume 2014, Article ID 659276, 8 pages
http://dx.doi.org/10.1155/2014/659276

Research Article

Fiber Bragg Grating-Based Performance Monitoring of Piles Fiber in a Geotechnical Centrifugal Model Test

Xiaolin Weng,[1] Jianxun Chen,[2] and Jun Wang[3]

[1] *Key Laboratory for Special Area Highway Engineering of Ministry of Education, Chang'an University, Xi'an, Shaanxi, China*
[2] *School of Highway, Chang'an University, Xi'an 710064, China*
[3] *China Railway First Survey and Design Institute Group Ltd., Xi'an 710064, China*

Correspondence should be addressed to Jianxun Chen; 416634900@qq.com

Received 7 August 2014; Revised 22 September 2014; Accepted 26 September 2014; Published 21 October 2014

Academic Editor: Hossein Moayedi

In centrifugal tests, conventional sensors can hardly capture the performance of reinforcement in small-scale models. However, recent advances in fiber optic sensing technologies enable the accurate and reliable monitoring of strain and temperature in laboratory geotechnical tests. This paper outlines a centrifugal model test, performed using a 60 g ton geocentrifuge, to investigate the performance of pipe piles used to reinforce the loess foundation below a widened embankment. Prior to the test, quasidistributed fiber Bragg grating (FBG) strain sensors were attached to the surface of the pipe piles to measure the lateral friction resistance in real time. Via the centrifuge actuator, the driving of pipe piles was simulated. During testing, the variations of skin friction distribution along the pipe piles were measured automatically using an optical fiber interrogator. This paper represents the presentation and detailed analysis of monitoring results. Herein, we verify the reliability of the fiber optic sensors in monitoring the model piles without affecting the integrity of the centrifugal model. This paper, furthermore, shows that lateral friction resistance developed in stages with the pipe piles being pressed in and that this sometimes may become negative.

1. Introduction

Based on such advantages as sound quality, bearing capacity, and low construction noise, the application of the prestressed concrete pipe pile has extended from the coastal, soft-soil regions to the inland, collapsible loess areas. Researchers, however, have recently focused more on the lateral friction resistance of pipe pile than on construction and inspection, which were of interest in early years. Shi [1] conducted a test by placing strain gauges in both ends of the pile and at the interfaces between different soil layers to measure both lateral friction resistance and bearing capacity. However, the thickness of the pipe influences this method to the extent of causing appreciable error due to the loss in friction resistance. Leng et al. [2] proposed embedding steel plates affixed to strain gauges during the prefabrication of pipe piles. Xiaokui [3] attempted to use Brillouin Optical Time Domain Reflectometry (BOTDR) to perform a load test on prestress high concrete (PHC) pipe piles that had already been hammered into the ground, but he found it impractical because of the excessively long sampling time. Again by use of BOTDR, Xing et al. [4] conducted a static load test on PHC pipe piles and succeeded in monitoring the load variation at each level. When Xu [5] performed strain monitoring, by placing FBG sensors on the surface of the static pressure piles, he succeeded in measuring end resistance and lateral friction resistance separately.

The advantages of optical fiber sensors over conventional monitoring techniques include immunity to electromagnetic interference, small size and lightweight construction, and access to different measurands, such as strain, temperature, vibration, and specified chemicals [6]. The optical fiber sensors can also be multiplexed, meaning that more than one sensor can be integrated along a single optical fiber. This multiplexing capability can enable a distributed mapping of the structure to be monitored [7].

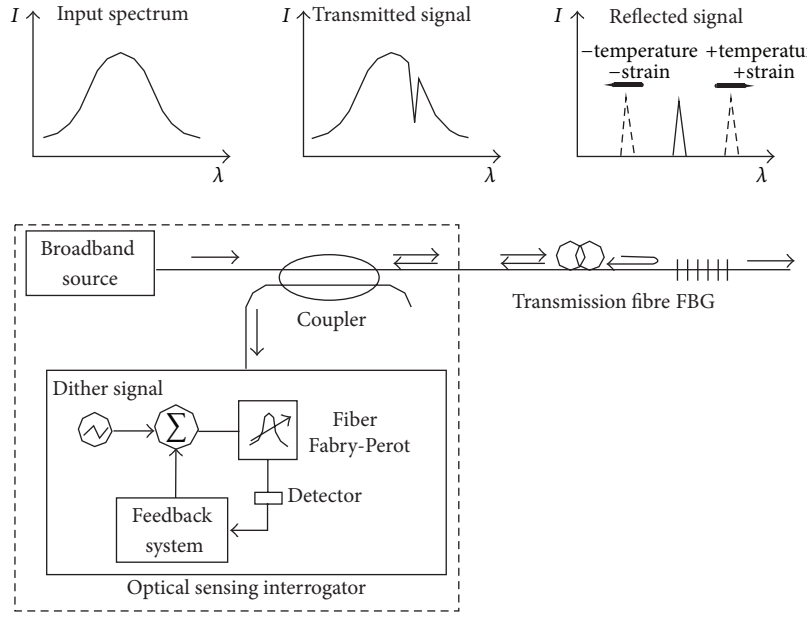

Figure 1: Strain and temperature sensing of an FBG sensor.

In the past decade, a series of fiber optic sensing technologies have been developed and applied to health monitoring of various geotechnical related structures, such as foundations, tunnels [8], caverns [9], and slopes [10]. Weng and Wang [11] reported the monitoring results of a physical model test of pavement instrumented by horizontally embedded FBG strain sensors. The response of the pavement due to differential settlement of embankment was presented and analyzed. Recently, Zhou et al. [12] utilized the same technology to perform in situ three-dimensional health monitoring of a pavement structure. In this testing process, researchers from Chang'an University used a 60 gt geocentrifuge and a subgrade model to study the performance of pipe piles in the collapsible loess foundation when placed under the load of widened subgrade. The centrifuge actuator was employed to simulate the pressing-in of the static pressure pile in the centrifugal field. Our researchers monitored the strain of piles using FBG sensors during different time periods—when piles were pressed in, subgrade put in service, or collapsibility generated within the loess foundation. The result of this study can provide reference for the design and construction of pipe piles in loess areas.

2. Bragg Grating Sensors

The sensing functioning of FBG was first discovered upon the formation of photogenerated gratings in germanosilicate optical fiber by Hill et al. [13]. Table 1 lists a feature comparison between the conventional and FBG sensors. The Bragg grating is written into a segment of germanium-doped (Ge-doped) single-mode fiber in which exposure to a spatial pattern of ultraviolet (UV) light forms a periodic modulation of the core refractive index. Figure 1 illustrates the working principle of an FBG sensor. According to Bragg's law, when a broadband source of light has been injected into the fiber, FBG reflects a narrow spectral part of light at a certain wavelength [14]:

$$\lambda_B = 2n_{\text{eff}}\Lambda, \tag{1}$$

where λ_B is the Bragg wavelength, typically 1510 to 1590 nm (1 nm = 10^{-9} m); n_{eff} is the effective core index of refraction; and Λ is the period of the index modulation.

Through physical or thermal elongation of the sensor segment, as well as through change in the fiber refractive index caused by photoelastic and thermo-optic effect, the Bragg wavelength will change linearly with strain and temperature. Considering a standard single-mode silica fiber, λ_B changes linearly with the applied strain $\Delta\varepsilon$ and temperature ΔT. This relationship is given by Kersey et al. [15] as

$$\frac{\Delta\lambda_B}{\lambda_{B0}} = c_\varepsilon\varepsilon + c_T\Delta T, \tag{2}$$

where λ_B is the original Bragg wavelength under strain free and 0°C condition, $\Delta\lambda_B$ is the variation in Bragg wavelength due to the applied strain and temperature, and c_ε and c_T are the calibration coefficients of strain and temperature. The typical strain and temperature accuracy of a bare FBG sensor are 1 $\mu\varepsilon$ and 0.1°C, respectively.

Because the FBG sensor is sensitive to both strain and temperature, separating the effect of temperature from the strain monitoring data becomes a key problem in data analysis. This temperature-compensation problem can be achieved by adding an FBG sensor or a conventional temperature sensor to the same temperature field. Once the temperature ΔT is measured, the mechanical strain can be corrected as follows [9]:

$$\Delta\varepsilon = \frac{1}{c_\varepsilon}\left(\frac{\Delta\lambda_B}{\lambda_B} - c_T\Delta T\right). \tag{3}$$

Table 1: Physical properties of the test soil.

Void rate	Saturation %	Dry density g/cm^3	Wet density g/cm^3	Natural water content %	Coefficient of collapsibility	Coefficient of Nonuniformity Cu	Coefficient of curvature (Cc)
18.62	1.85	1.39	1.57	12.84	0.086	8.02	1.35

Figure 2: Model pipe pile with sensors packaged.

Figure 3: Model pipe pile with sensors packaged.

The FBG package is one of the key points in strain monitoring. Only 250 μm cross, the bare fiber is very thin and exerts little influence on the monitored structure. In this test, fibers were adhered directly to the surface of the seamless steel pipe using ALTECO epoxy resin. As shown in Figure 2, twelve FBG sensors are symmetrically arranged from the point 15 mm below the top in two lines along the steel pipe at an interval of 20 mm. Readings from the pair of sensors at the same height will be averaged (the six pairs are numbered FBG1–6 from the top down). Figure 3 shows a pipe pile model with sensors already packaged. The sensors are affixed in parallel with the steel pipe so that they develop the same strain. A dynamic optical demodulator, SM130 of Micron Optics, is applied to measure the variation of wavelength of the FBG. The SM130 is a high-speed, heavy-duty measuring system designed primarily for use in mechanical testing. Capable of handling multiple sensors, this system applies to the measurement of strain, temperature, pressure, acceleration, and more. The SM130 has a top scan frequency of 1 kHz, which well meets the requirement of strain measurement at various pressing rate of piles.

3. Centrifugal Experiments

The soil for this test was taken from the suburb of Xianyang, which has an optimum water content of 14.0% and a maximum dry density of 1.83 g/cm^3 as the result of compaction testing. According to the consolidated undrained test, conducted under different levels of compression, the cohesion and the internal friction angle of the sample soil are, respectively, obtained as 51 kPa and 22°. Table 1 shows the other physical properties of the test soil.

The model test is designed according to the centrifuge actuator. The model is prepared in box sizes 740 mm × 560 mm × 460 mm on a scale of 1/60, as shown in Figure 3. The foundation contains a bottom layer Q3 of loess and a top layer Q1 of original soil, both placed and compacted in layers. The compaction intensity for Q3 is adjusted to obtain a desired elastic modulus. The original soil for Q1 is used in order to maintain collapsibility of the foundation. Dry silver sand is placed between the soil and the model box to reduce the error caused by cracking. Both the new and old 110 mm high subgrades are placed and compacted in as many layers as possible to minimize foundation damage.

At the beginning of the test, the placement of the old subgrade is simulated. Following this, the centrifuge is run at its top acceleration, 60 g, for a long period to ensure the old foundation soil material consolidation fully. After that, researchers stop the centrifuge, cut steps on the slope of the old subgrade, as shown in Figure 3, and then start the foundation treatment by using pipe piles. These seamless steel pipe piles—170 mm in length, 8 mm in diameter, and 1 mm in thickness—are arrayed at an interval of 30 mm. They represent prototypes that are 10 m in length, 480 mm in diameter, and 60 mm in thickness and are arrayed at an interval of 1.8 m, as shown in Figure 4. Coarse sand is chosen for the bedding cushion. After the foundation treatment is complete, the new subgrade is placed in layers after the completion of foundation treatment. Next, the centrifuge is run in six steps, to its top acceleration of 60 g, with runtimes of, respectively, 43.2, 10.8, 4.8, 2.7, 1.7, and 1.2 minutes. This simulates new subgrade placed in six layers with duration of three days for each. The centrifuge is run at 60 g for 438 minutes, which is equivalent to three years of service of the new subgrade; the strain of piles is monitored during this period. Later, the new subgrade is humidified to cause collapsible deformation. Strain of the piles is again monitored.

3.1. Design of the Pipe Pile. The pipe pile for the model test, in accordance with the similarity theory, is made of the same

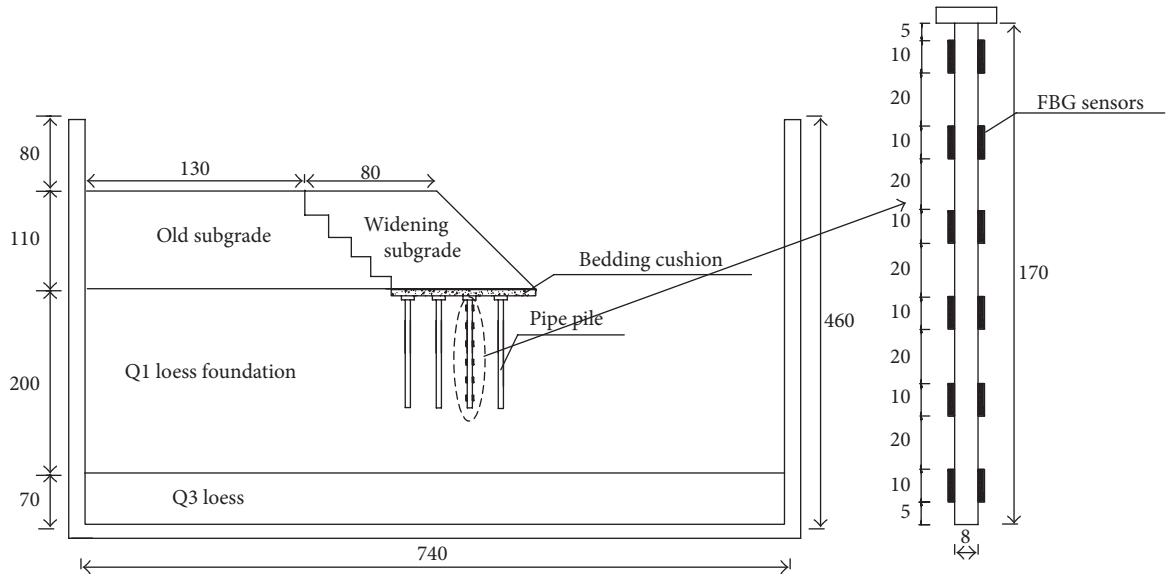

Figure 4: Illustration of the model test (unit: mm).

material (i.e., concrete and reinforcing steel) used in the real one. However, the similarity theory also determines the diameter of the model pipe pile to be 10 mm (600/60), which is almost impossible to obtain by casting concrete; therefore, a substitute material is needed. Hence the 10 mm seamless steel pipe is applied in this test to simulate the real pipe pile, which is 10 m in length, 60 cm in diameter, and 30 cm in thickness with an elastic modulus of 60 GPa. Figure 5 shows the result of the unconfined compression test of the steel pipe. By fitting the stress-strain curve, an elastic modulus of 55 GPa is obtained for the model pile, which achieves a similarity ratio of 1 to that of the real one. This has effectively reflected the feasibility of replacing the concrete pipe with seamless steel pipe.

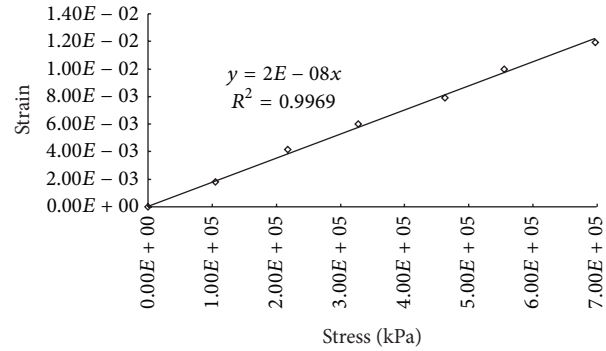

Figure 5: Result of unconfined compression test of seamless steel pipe.

3.2. Pressing-In of the Pipe Piles. Simulating the construction of jacked pipe piles, the pipe pile is pressed in within the centrifugal field by the 60 g ton geocentrifuge actuator of Chang'an University, as shown in Figure 6. The actuator is composed of the mechanical system and the electric system; the former includes the robotic arm and model box while the latter includes the computer and monitoring systems along with the power control cabinet. The actuator has four axes (i.e., X, Y, Z, and C), each independently driven by a motor to achieve four-axis positioning. As Figure 7 shows, it also includes a tool designed to press piles. It takes nine times to press the whole 170 mm long model pile into soil. With the exception of the final time, the pile goes 20 mm deeper each time; it has only 10 mm to go the last time. The model piles are arranged at different ratio S/d (S is the distance between piles and d is the pile diameter) of 1, 2, and 3 to evaluate the friction resistance of collapsible loess foundation against various pile arrangements. Figure 8 shows model piles being pressed in by the actuator, and Figure 6 shows the model piles already driven in place at an S/d ratio of 4.

3.3. Water Log Infiltration System. A plexiglass box with two chambers was used in the experimental test setup to simulate water spill into soil from an underground storage tank, as shown in Figure 9. This type of experimental test setup was first used by Esposito and Allersma [16] and Pasha et al. [17]. The setup included a tank and a supply of the flushing liquid, along with a dispenser box to inject the flushing liquid into loess soil. The tank was fixed onto the centrifuge platform, and the dispenser was placed on top of soil in the strongbox. The chamber was connected to the air-pressure supply. At the appropriate time, when the centrifuge was spinning, air pressure was applied to the tank to push the required volume of water into the dispenser. The dispenser was refilled many times by this process until the total required flushing volume had been injected.

4. Results and Discussion

The lateral friction resistance of the pipe piles is shown in Figure 10. This reveals that the pipe pile behaves in

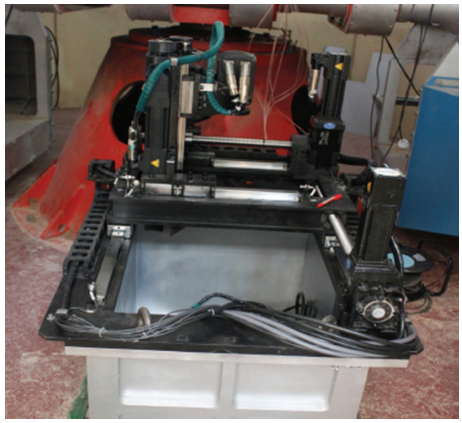

Figure 6: Centrifuge actuator.

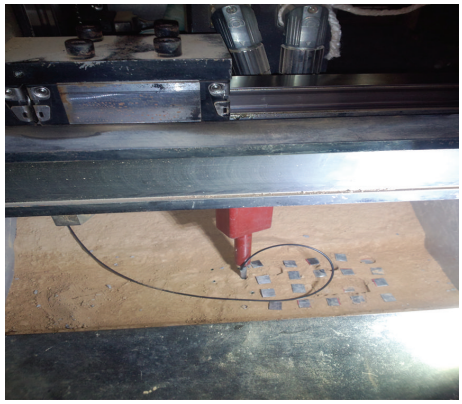

Figure 7: Pipe piles press-in process.

Figure 8: Finish of jacked pipe piles ($S/d = 4$).

the exact way of a friction pile in the loess foundation. Before subgrade filling, the pile bears only its dead load and the lateral friction resistance stays at a low level, with a maximum value of approximately 20 kPa. Shortly after the subgrade filling, the pipe pile bears the most substantial part of the subgrade load and moves down, relative to the surrounding soil. The lateral friction resistance increases substantially, up to 80 kPa near the top, and decreases along the way, down to a minimum of 40 kPa. When one year has passed since subgrade filling, the lateral friction resistance begins to show a sharp decrease, caused by the compression of the soil body between the piles; this compression, in turn, results from its participation in bearing subgrade load. The pipe pile exhibits a negative correlation between the lateral friction resistance and the ratio of S/d. The smaller the ratio, the greater the friction resistance, as the soil between the piles is more intensively compressed. The study results are basically similar with Kong et al. [18] and Huang et al. [19].

Figure 11 shows the lateral friction resistance of the pipe pile in wetted, collapsible loess foundation. Although the pipe pile treatment neutralizes the collapsibility of the original loess foundation to a certain degree, collapse still occurs in various degrees—depending on the intensity and duration of water soaking on the surface—and causes negative friction. The longer the soaking time, the greater the negative friction. The negative-friction resistance decreases along the way down, eventually reaching a neutral point. According to Figure 11, after three days of water soaking, negative friction develops within the area 20 mm below the top of pile. As soaking time increases, the negative friction also increases, and the neutral point moves gradually down and finally stops at a certain depth. For example, after ninety days of water soaking, the ratio between the depth of neutral point and the length of pipe pile is $0.35 \sim 0.41$. According to Figure 11(a), the negative friction increases only slightly after ninety days of soaking beyond its friction after three days of soaking. In comparison, this negative friction in Figure 11(c) goes up to 45 kPa, which indicates that dense arrangement of piles can improve the intensity of compression, greatly reducing the collapsibility of soil.

5. Conclusions

The fiber Bragg grating sensor offers distinct advantages, such as its small size and limited influence on structure or over the other instruments in the skin friction monitoring of pipe piles. The model test is successfully performed using an FBG sensor that exhibits high sensitivity and resolution, even when placed in centrifugal field. Jacked pipe piles in centrifugal field can be accomplished by use of the actuator of the Chang'an University geocentrifuge. The strain variation during the pressing-in of pile was monitored by the FBG sensors, which show that the pipe pile exhibits a negative correlation between the lateral friction resistance and the ratio of S/d. The smaller the ratio, the greater the friction resistance, as the soil between the piles is more intensively compressed. Dense arrangement of piles can improve the intensity of compression, greatly reducing the collapsibility of soil.

Conflict of Interests

The authors declare that there is no conflict of interests regarding the publication of this paper.

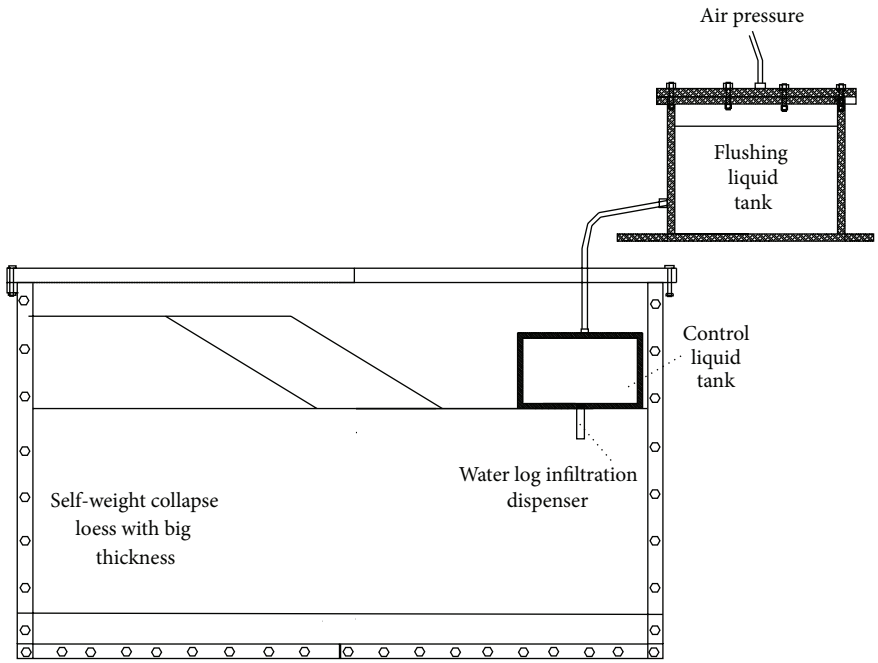

Figure 9: Schematic of centrifuge experiments setup for water log infiltration.

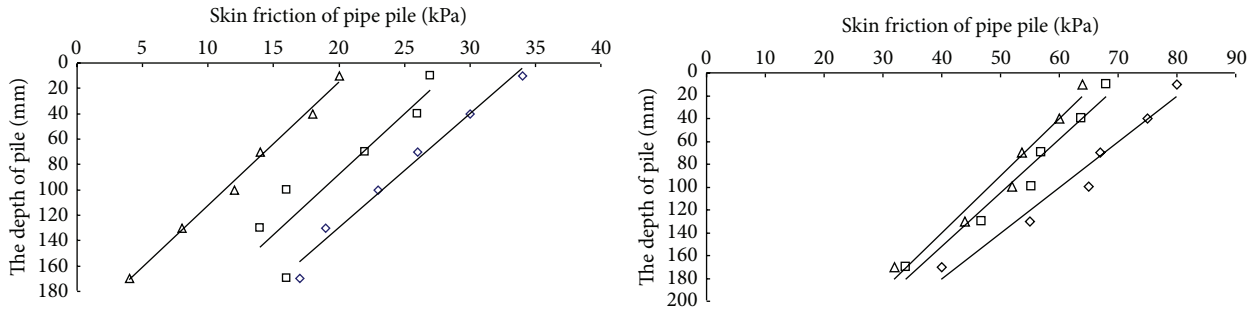

(a) The completion of pipe pile construction

(b) The completion of subgrade filling

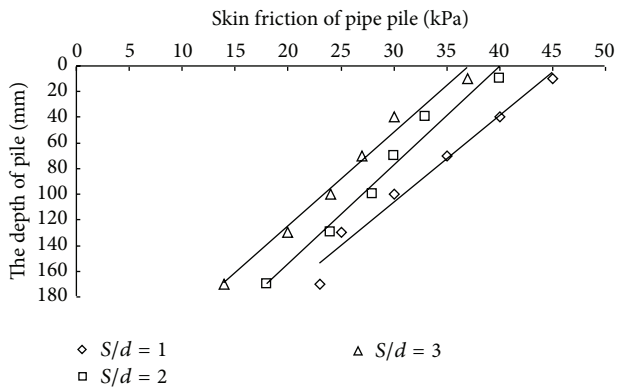

(c) 1 year after construction

Figure 10: Skin friction distributions along the pile depth.

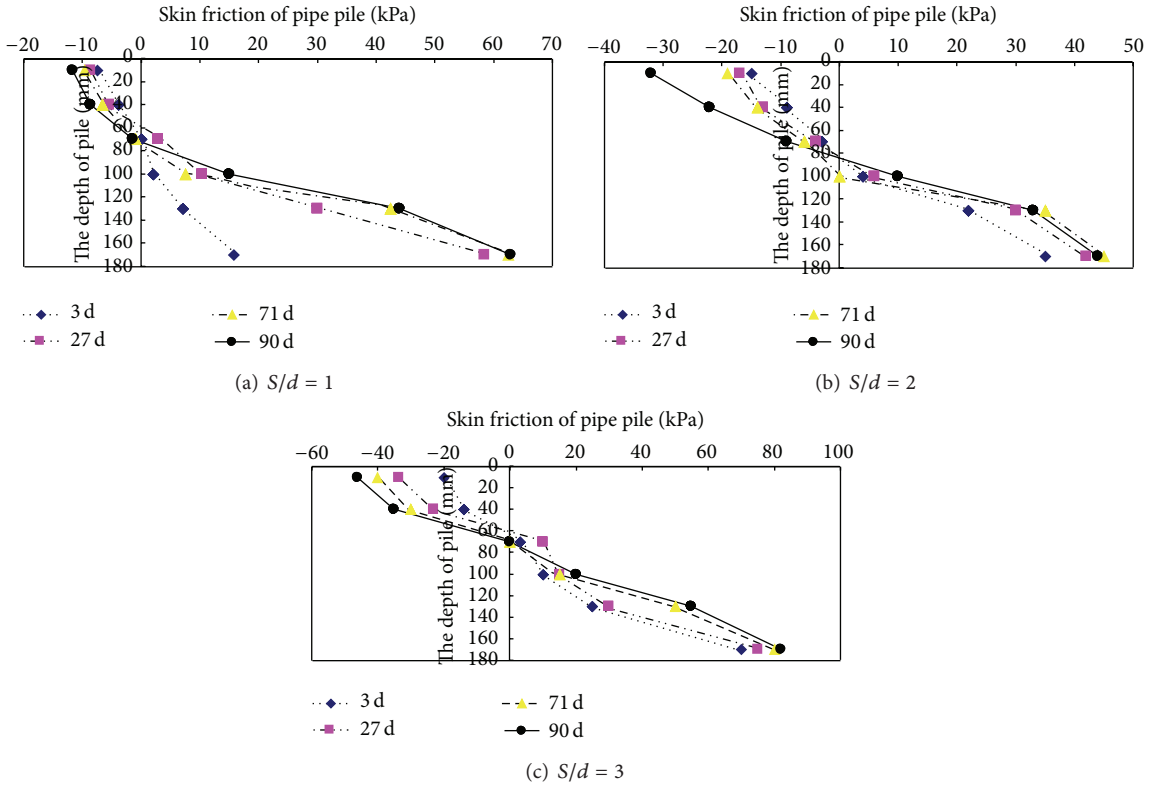

FIGURE 11: Skin friction distributions along the pile depth during water log infiltration.

Acknowledgment

This work was supported by the National Natural Science Foundation of China (Grants nos. 51008032 and 51378004).

References

[1] F. Shi, "Experimental research on load transfer mechanism of pretensioned high strength spun concrete piles," *Chinese Journal of Geotechnical Engineering*, vol. 26, no. 1, pp. 95–99, 2004.

[2] W. Leng, L. Wei, and Z. Hua, "Experimental study on subgrade reaction under raft foundation restressed with unbonded tendon," *Chinese Journal of Geotechnical Engineering*, vol. 22, no. 4, pp. 456–460, 2000.

[3] Y. Xiaokui, "Research on the testing of pile based on distributed optical fiber monitoring sensing technique," *Electric Power Survey and Design*, no. 6, pp. 12–16, 2006.

[4] H.-F. Xing, H.-W. Zhao, G.-B. Ye, and C. Xu, "Analysis of engineering characteristics of PHC pipe piles," *Chinese Journal of Geotechnical Engineering*, vol. 31, no. 1, pp. 36–39, 2009.

[5] J. Xu, *Study on the pile resistance and the optical fiber method of the jacked pile stress [Ph.D. thesis]*, Qingdao Technological University, Qingdao, China, 2011.

[6] G. Kister, D. Winter, Y. M. Gebremichael et al., "Methodology and integrity monitoring of foundation concrete piles using Bragg grating optical fibre sensors," *Engineering Structures*, vol. 29, no. 9, pp. 2048–2055, 2007.

[7] R. L. Idriss, M. B. Kodindouma, A. D. Kersey, and M. A. Davis, "Multiplexed Bragg grating optical fiber sensors for damage evaluation in highway bridges," *Smart Materials and Structures*, vol. 7, no. 2, pp. 209–216, 1998.

[8] N. Metje, D. N. Chapman, C. D. F. Rogers, P. Henderson, and M. Beth, "An optical fiber sensor system for remote displacement monitoring of structures—prototype tests in the laboratory," *Structural Health Monitoring*, vol. 7, no. 1, pp. 51–63, 2008.

[9] W. S. Zhu, Q. B. Zhang, H. H. Zhu et al., "Large-scale geomechanical model testing of an underground cavern group in a true three-dimensional (3-D) stress state," *Canadian Geotechnical Journal*, vol. 47, no. 9, pp. 935–946, 2010.

[10] B.-J. Wang, K. Li, B. Shi, and G.-Q. Wei, "Test on application of distributed fiber optic sensing technique into soil slope monitoring," *Landslides*, vol. 6, no. 1, pp. 61–68, 2009.

[11] X. L. Weng and W. Wang, "Influence of differential settlement on pavement structure of widened roads based on large-scale model test," *Journal of Rock Mechanics and Geotechnical Engineering*, vol. 3, no. 1, pp. 90–96, 2011.

[12] Z. Zhou, W. Liu, Y. Huang et al., "Optical fiber Bragg grating sensor assembly for 3D strain monitoring and its case study in highway pavement," *Mechanical Systems and Signal Processing*, vol. 28, pp. 36–49, 2012.

[13] K. O. Hill, B. Malo, F. Bilodeau, D. C. Johnson, and J. Albert, "Bragg gratings fabricated in monomode photosensitive optical fiber by UV exposure through a phase mask," *Applied Physics Letters*, vol. 62, no. 10, pp. 1035–1037, 1993.

[14] W. W. Morey, G. Meltz, and W. H. G. Glenn, "Fiber optic bragg grating sensors," in *SPIE Fiber Optic and Laser Sensors VII*, vol. 1169 of *Proceedings of SPIE*, pp. 98–107, Boston, Mass, USA, 1989.

[15] A. D. Kersey, M. A. Davis, H. J. Patrick et al., "Fiber grating sensors," *Journal of Lightwave Technology*, vol. 15, no. 8, pp. 1442–1463, 1997.

[16] G. Esposito and H. G. B. Allersma, "Centrifuge simulation of in-situ contamination removal," in *Proceedings of the International Symposium on Physical Modelling and Testing in Environmental Geotechnics*, pp. 141–148, La Baule-Escoublac, France, May 2000.

[17] A. Y. Pasha, L. Hu, J. N. Meegoda, E. Aflaki, and J. Du, "Centrifuge modeling of in situ surfactant enhanced flushing of diesel contaminated soil," *Geotechnical Testing Journal*, vol. 34, no. 6, pp. 209–216, 2011.

[18] G.-Q. Kong, Q. Yang, P.-Y. Zheng, and M.-T. Luan, "Model tests on negative skin friction for inclined pile considering time effect," *Chinese Journal of Geotechnical Engineering*, vol. 31, no. 4, pp. 617–621, 2009.

[19] X. F. Huang, Z. H. Chen, S. Ha, S. G. Xue, and S. X. Sun, "Research on bearing behaviors and negative friction force for filling piles in the site of collapsible loess with big thickness," *Chinese Journal of Geotechnical Engineering*, vol. 29, no. 3, pp. 338–346, 2007.